北海道大学地球物理学研究報告
Geophysical Bulletin of Hokkaido University, Sapporo, Japan
No. 68, March 2005, pp. 71−90

Doppler Radar Observations of Blocked Airflow off the Southeast Coast of the Kii Peninsula in Japan

Yasushi FUJIYOSHI
Institute of Low Temperature Science, Hokkaido University, Sapporo, Japan
FRCGC/JAMSTEC, Yokohama, Japan
Hisamichi TANAKA*
Institute of Hydrospheric-Atmospheric Science, Nagoya University, Nagoya, Japan
Masayuki KAWASHIMA
Institute of Low Temperature Science, Hokkaido University, Sapporo, Japan
Ken-ichi MARUYAMA
National Research Institute of Earth Science and Disaster Prevention, Tsukuba, Japan
and
Takao TAKEDA
Prof. Emeritus, Nagoya University, Nagoya, Japan
(Received December 20, 2004)

A dual-Doppler radar system was deployed on the eastern side of the Kii Peninsula from June to October 1993, and observed a low-level stratiform radar echo that persisted off the coast for more than 7 hours in a stable atmosphere on 7 October. Analysis of three-dimensional wind fields confirmed the presence of a blocked airflow in the upstream region of the mountains. The blocked airflow extended about 45 km off the coast; it was 2 km deep near the coast, but its thickness decreased with increasing distance from the coast. The mean slope angle of the boundary between the blocked and the environmental airflows was about 2.5 degrees. As the environmental wind speed increased, the horizontal extent of the blocked airflow decreased and the vertical extent increased. These observations are consistent with results from a mesoscale numerical model.

I. Introduction

Orographically modified wind fields over ocean and land greatly influence the development and modification of clouds that cause locally heavy precipitation at many locations. Among them, the southeastern Kii Peninsula, located in the middle part of Honshu Island of

*Present affiliation: Communication Systems Center, Mitsubishi Electric Corporation, Amagasaki, Japan

Japan (Fig.1), experiences some of the heaviest rainfall in Japan, and many researchers have studied its formation mechanisms. Staff members of Tokyo University (1969, 1970) suggested that orographic lifting is mainly responsible for the heavy rainfall in this mountainous area. Sakakibara and Takeda (1973) noted the importance of microphysical interactions between raindrops in traveling convective clouds and cloud droplets in orographic layer clouds. Radar data used by researchers (e.g., Yanagisawa et al., 1974; Fujiwara et al., 1974; Takeda and Takase, 1980; Sakakibara, 1981) have highlighted the importance of low-level convective clouds that form repeatedly over the same area offshore and subsequently move inland over the mountains.

Shiino (1976) used radiosonde observations from Shionomisaki taken during heavy rainfall events at Owase (their locations are shown in Fig. 1) to simulate convective clouds with a one-dimensional cumulus convection model. His result demonstrated that shallow convective clouds are able to develop over regions of horizontal convergence. Takeda et al. (1976) noted the importance of microphysical interactions between traveling cumulonimbi and small clouds that formed near Owase. The same study further suggested that both cloud systems are modified or enhanced by orographically-forced mesoscale horizontal convergence on the windward side of the mountains when easterly winds dominate. Saito et al. (1994) simulated airflow over the southeastern Kii Peninsula with a three-dimensional, anelastic version of the nonhydrostatic model. In their dry model, low-level convergence due to upstream blocking by the mountains affects the orographic enhancement of the convective rainband over the sea on the windward side of the Kii Peninsula. Upstream blocking of airflow is also suggested to significantly enhance local heavy rainfall in other countries (e.g., Kuo and Chen, 1990; Carbone et al., 1995 and 1998; Bousquet and Smull, 2003) and snowfall (e.g., Fujiyoshi, 1992; Saito et al., 1994; Kodama et al., 1999).

In Japan, several dual Doppler radar studies have described airflow modified by orography (Fujiyoshi et al., 1996; Nakai et al., 1998; Seko et al., 1999; Kanada et al., 2000; Yoshihara et al., 2004; Kawashima and Fujiyoshi, 2005). Over the southeastern Kii Peninsula, however, 3D Doppler wind fields were not revealed until a dual-Doppler radar system from Nagoya University was deployed between June and October 1993. The existence of a horizontal convergence zone about 10 km offshore, as inferred by average horizontal winds observed in the dual-Doppler radar system, was suggested in our previous paper (Kanada et al., 1999). Although they discussed the intensification of traveling rainbands near the convergence zone and their orographic modification, the structure of the convergence zone itself was not. In addition, it was unclear whether the convective clouds modified the environmental airflow, or not.

The height and shape of the boundary between blocked and upstream airflow are important factors to trigger, modify or enhance the convection within the conditionally unstable or unstable upstream atmosphere. As Smull et al. (2001) pointed out, an underestimation by numerical simulations of the depth and extension of the blocked airflow causes unrealistically large and misplaced forecast rain amounts in the mountainous area. Once precipitation begins, some convective clouds and/or rainbands can be stationary and long-lasting by the interaction between clouds and the blocked airflow. It is almost impossible to distinguish between wind fields modified by orography and by the convective clouds during heavy rainfall. Therefore, we have to observe wind fields before heavy rainfall occurs to study the structure of the blocked airflow. So far, however, there has been no report on the 3D wind fields formed just before a rainband approaches to the convergence zone.

On 7 October 1993, low-level stratiform radar echoes repeatedly appeared over a period of more than 7 hours off the coast of the Kii Peninsula before rainbands associated with Typhoon 9319 approached to the coast. This fact implies persistent low level convergence there in a stable atmosphere (as shown in Section 2) that caused updrafts. Since the updraft air brought light precipitation, we were able to retrieve wind fields based on dual-Doppler radar observations. This study is the first to confirm the existence and show a detailed 3D structure of blocked airflow prior to heavy rainfall, in other words, before convective clouds affect and modify the blocked airflow.

II. Observations

X-band Doppler radars were deployed at Wagu and Fujisaka Pass on the eastern side of the Kii Peninsula. Fujiyoshi et al. (1998) include the detailed radar characteristics. Figure 1 shows the two radar sites, radar coverage (two circles), the upper air sounding station (Shionomisaki) and the topography. Three-dimensional scans of radar data were recorded every 7 minutes on a Cartesian grid with a resolution of 0.5 x 0.5 km in the horizontal and 0.25 km in the vertical. The Fujisaka radar was at an altitude of 0.55 km, so the lowest level of data was at 0.75 km.

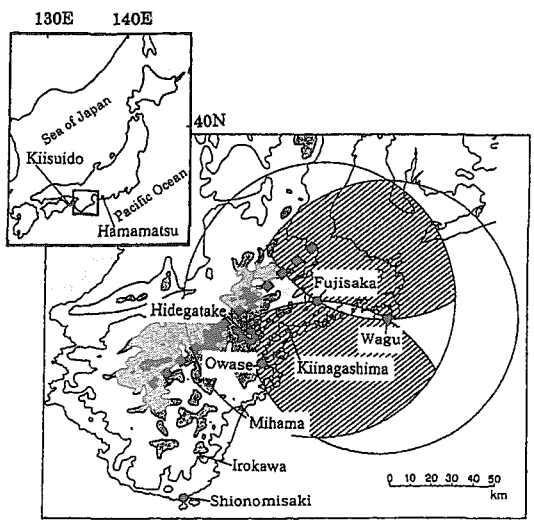

Fig. 1. Topography of the Kii Peninsula and observation ranges of two Doppler radars (from Kanada et al., 1999)

1 Classification of radar echo pattern

Ten rainfall events were observed between July and October 1993, comprising a total operation period of 150 hours. Radar data from Nagoya Meteorological Observatory facilitated the classification of radar echo patterns into three types. Typical examples of following three types of radar echo patterns are shown in Fig. 2.

(1) Mountain type (M-type: three cases of ten) (Fig. 2a) : Radar echoes appeared only over the mountains. The cases analyzed by Staff members of Tokyo University (1969, 1970) and Sakakibara and Takeda (1973) belong to this M-type. Orographic lifting of air parcels along the mountain slope is suggested to be mainly responsible for the rainfall in the mountainous area.

(2) Landing type (L-type: six cases of ten) (Fig. 2b): Radar echoes appeared (or developed) over sea and subsequently moved inland over the mountains. Takeda et al. (1976), Takeda

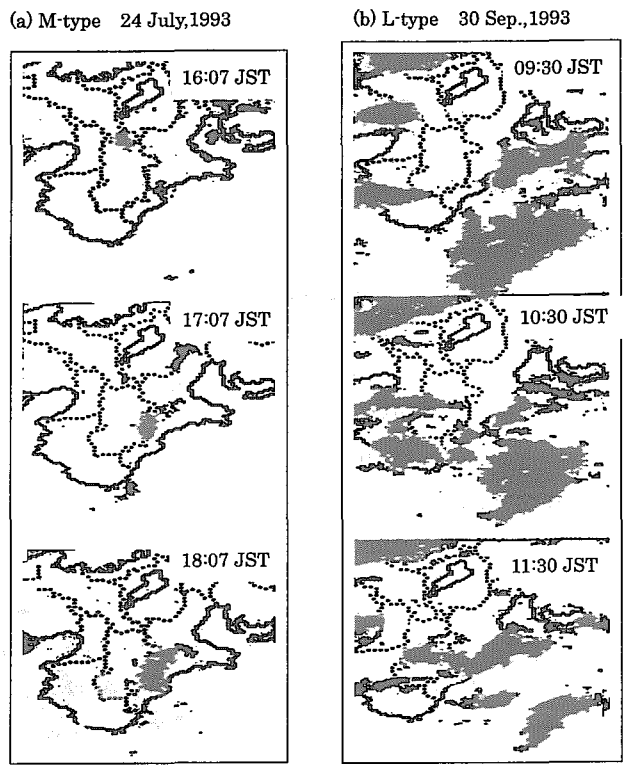

Fig. 2. (a) PPI radar echo patterns of M-type (from 16:07 to 18:07 on 24 July, 1993); (b) PPI radar echo patterns of L-type (from09:30 to 11:30 on 30 September, 1993)

and Takase (1980), and Kanada et al. (1999) investigated these L-type echoes.

(3) Coast type (C-type: one case of ten) (Fig. 3): Weak echoes persisted over the sea and the coast.

2 Case selected for analysis

Typhoon 9319 moved northeastwards about 900 km offshore of the Kii Peninsula at 21 JST on 6 October (Fig. 4) and approached the radar sites (all times are JST; JST=UTC+9 hr). The radar echoes of the typhoon rainbands merged with C-type echoes at around 12:30 on 7 October. C-type echoes were observed off the coast of the Kii Peninsula from 05:30 to 13:00 on 7 October. Because these echoes were not convective and were very weak (less than

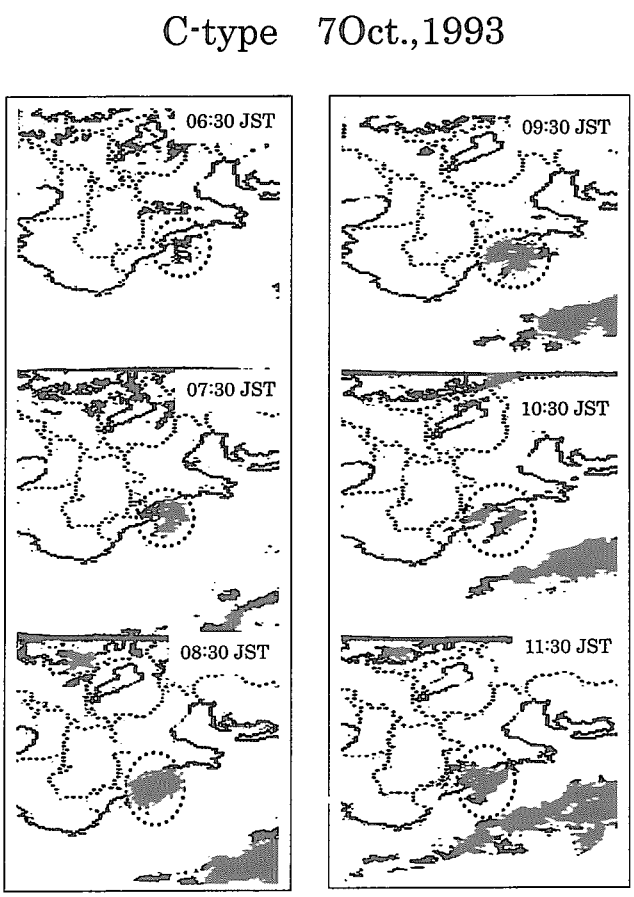

Fig. 3. PPI radar echo patterns of C-type (from 06:30 to 11:30 on 7 October, 1993).

20 dBZ; < 1 mm hr^{-1}) as shown in next section, the environmental airflow is far more likely to have been affected by the orography than by the clouds. Therefore, this case presents a good opportunity to study the effect of orography on offshore, upstream, wind fields.

III. Time-averaged structure

Figure 3 shows the weak radar echoes that persisted off the coast for more than 7 hours, suggesting the existence of a long-lived convergence zone that forced a weak updraft off the coast. Time-height cross-sections of the horizontal wind speed and direction above Fujisaka (Fig. 5) were made using the velocity azimuth display (VAD) method (Browning and Wexler, 1968). These cross-sections helped to study the change with time of the wind fields. A vertical profile of horizontal winds was not able to be derived above Wagu because there were no radar echoes there. The wind direction above Fujisaka did not change largely between 06:00 and 14:00; it was almost constant in the layer between 1.0 and 2.5 km during the first half of the period. Therefore, the mean vertical and horizontal structures of the convergence zone was studied using radar echo intensity and wind fields averaged over the period 06:30-09:20 (shown by arrows in Fig. 5).

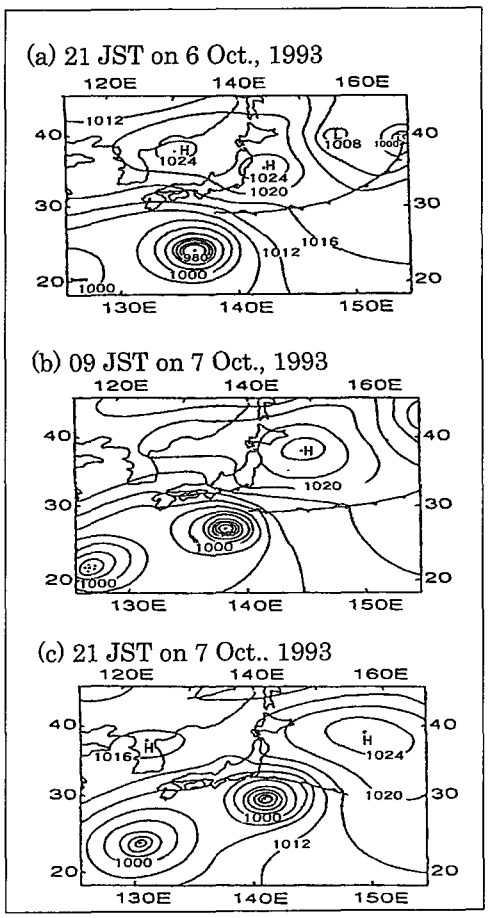

Fig. 4. Surface weather maps from 21 JST on 6 October to 21 JST on 7 October, 1993.

Time-averaged vertical profiles of wind components (U [eastward] and V [northward]) and horizontal wind speeds show nearly the same structures at Fujisaka as those from upper air sounding data at Shionomisaki (Fig. 6). At both sites, a local maximum wind speed occurred near 1.7 km and the wind direction veered from ENE to SW with height. This fact indicates that these features were common over at least the eastern and southern Kii Peninsula. Upper air soundings at Shionomisaki

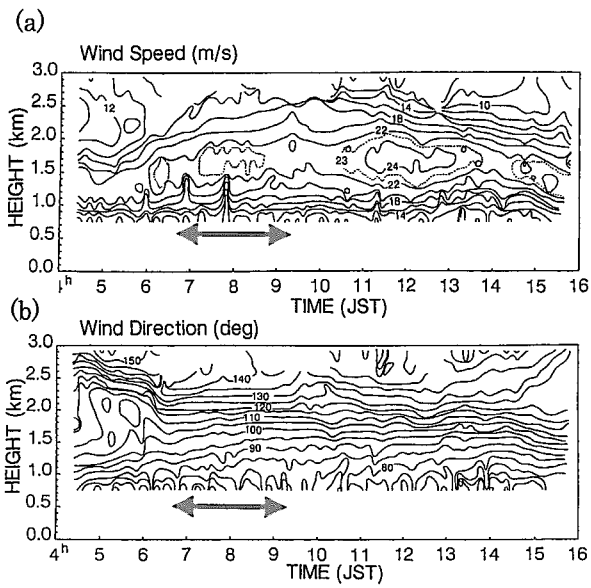

Fig. 5. Time-height cross-sections of the horizontal wind speed (a) and direction (b) above Fujisaka from 04:20 to 15:40 JST on 7 October, 1993.

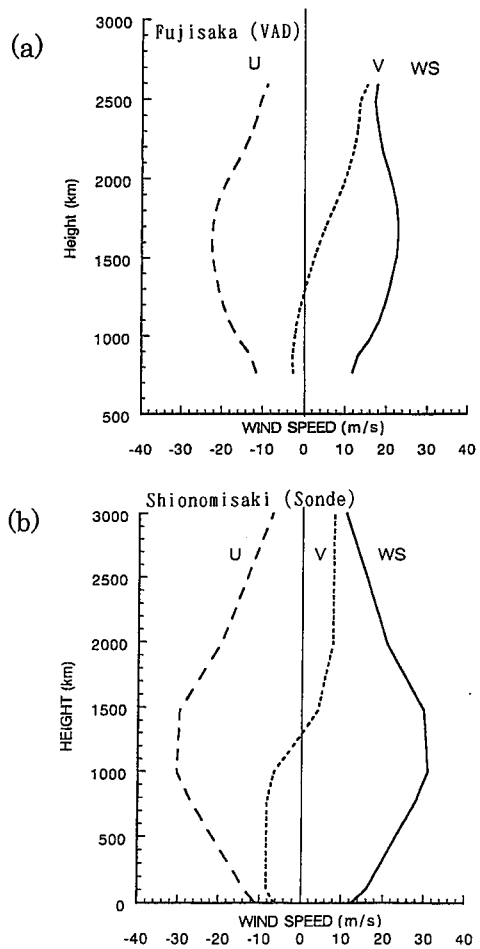

Fig. 6. Time-averaged (06:30−09:20 JST) vertical profiles of wind components (U and V) above Fujisaka (a), and those from upper air sounding data (09 JST) at Shionomisaki (b).

revealed a very humid and stable lower atmosphere (Fig. 7).

Figure 8 shows horizontal distributions of time-averaged radar echoes and wind fields. The clouds were warm rain clouds, because the radar echo top was at less than 2 km and thus below the freezing level (4.5 km). The time-averaged wind direction at a height of 0.75 km was northeasterly and easterly just off and off the coast, respectively. The maximum radar echo intensity appeared about 10 km off the coast. Figure 9 shows the horizontal distributions of the time-averaged radar echo and wind speed at a height of 0.75 km. Wind speeds near the coast were 10 m s^{-1} slower than offshore. The eastern boundary of radar echo defined by 4dBZ and isotachs were parallel not with the coastline, but with the mountain ridge in the downwind side (see thick dotted line in Fig. 1). This feature is consistent with that of the simulated blocked airflow by Saito et al. (1994) and ours (see Section 5).

The radar echo intensity and wind speeds in Fig. 9 on the X-axis (X=0−80 km) were averaged on the Y-axis between Y=0−9 km to yield an X-Z cross section of the mean radar echo and wind fields, which enabled an examination of their vertical structure. The X-axis of this rectangular box was nearly perpendicular to the isotachs. The place of the box was decided so as to include the region where the radar echo intensity and the level of echo top were the maximum (see Fig. 8). Figure 10 shows vertical cross sections of the mean radar

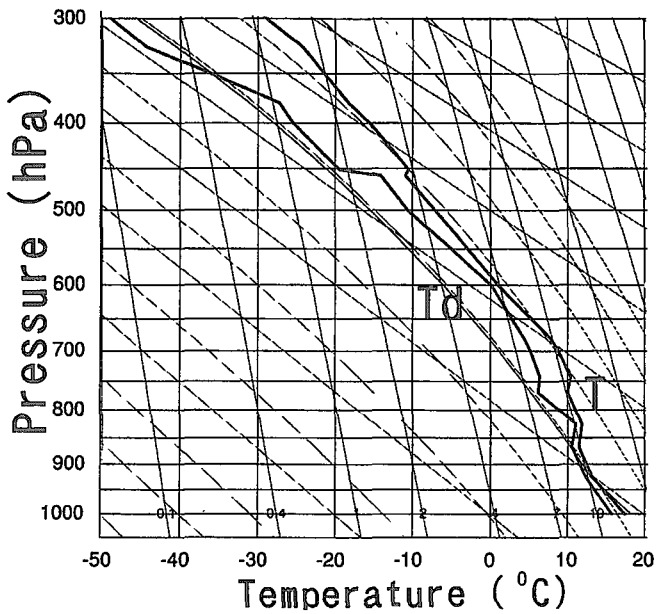

Fig. 7. Upper air sounding data (09 JST on 7 October) at Shionomisaki.

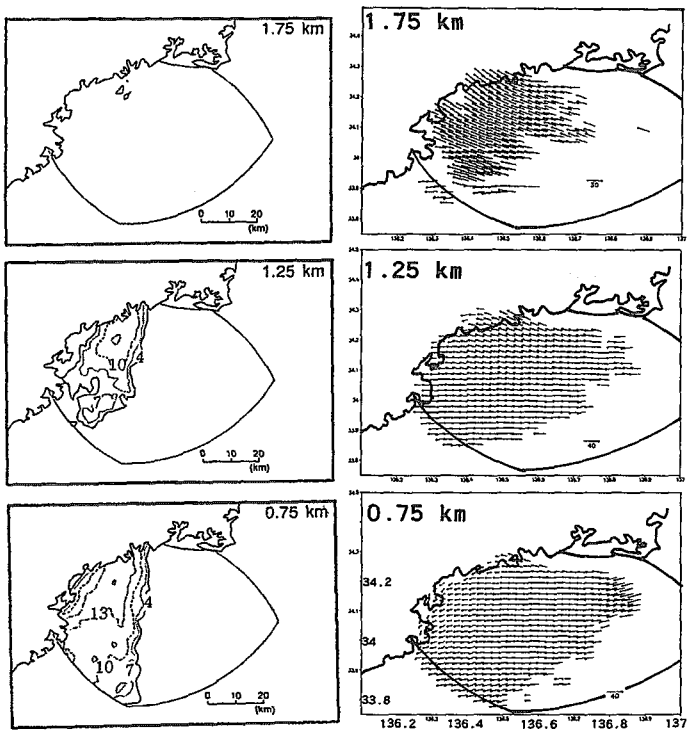

Fig. 8. Horizontal distributions of time-averaged radar echoes (dBZ) and wind vectors.

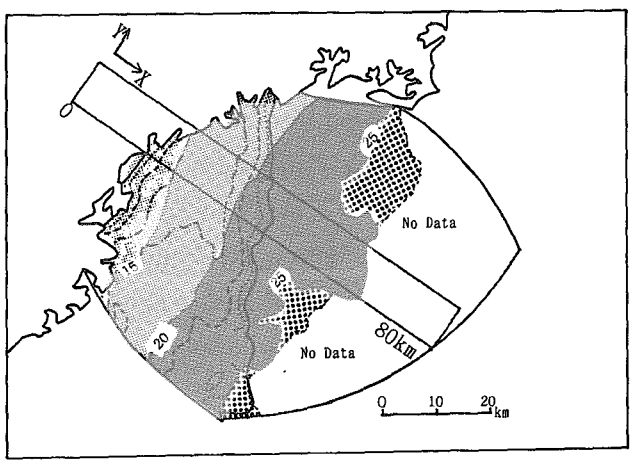

Fig. 9. Horizontal distributions of the time-averaged radar echo (contour, same with Fig.8) and wind speed (shaded) at a height of 0.75 km. The attached numbers mean horizontal wind speed.

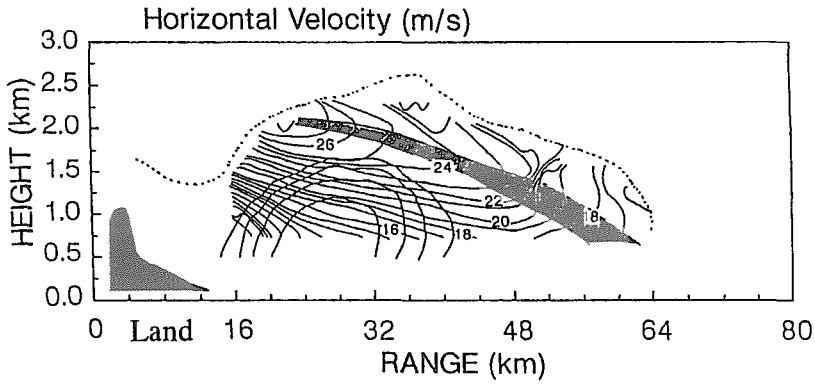

Fig. 10. Vertical cross section of the mean radar echo and horizontal velocity along the X-axis in Fig. 9.

echo and horizontal velocity. The height of the boundary between the lower weak airflow region and the upper environmental airflow (indicated by a thick shaded band), where vertical gradient of horizontal wind velocity changed largely, increased closer to the coast (about 2. 0 km in depth). The mean slope of this boundary was about 2.5 degrees. Horizontal wind speeds started to weaken around X=55 km; orography affected the wind fields more than 45 km off the coast. The Doppler radar detected signals above noise level below the dotted line. The height of the dotted line began to increase around 64 km (about 50 km offshore), indicating the growth of raindrops within the uplifting air along the boundary. These results support the conclusion of Saito et al. (1994) that upstream blocking by mountains causes upward air motion and a corresponding formation of low level weak echoes.

The height of the dotted line began to decrease around 36 km, which suggests that upward air motion was the strongest there. It rapidly descended and radar echo intensity was weak (see also Fig. 8) near the sea coast (around 16 km), where wind direction changed from easterly to northeasterly, suggesting evaporation of raindrops and the presence of downward air motion. The increase of the echo top along the slope of the mountain would be caused by the forced updraft by the mountain. Unfortunately, the radar echo intensity there was too weak and ground clutter contamination was too strong for reliable wind fields to be retrieved. Numerical simulation results will be used to discuss these features in Section V.

IV. Change with time of horizontal wind speeds and weak radar echo locations

Although the weak radar echo persisted in nearly the same region, its location and intensity varied slowly with time. Figure 11a shows the time-range cross section of echo intensity at a height of 1.0 km within the box of Fig. 9. Radar echoes appeared at around 05:

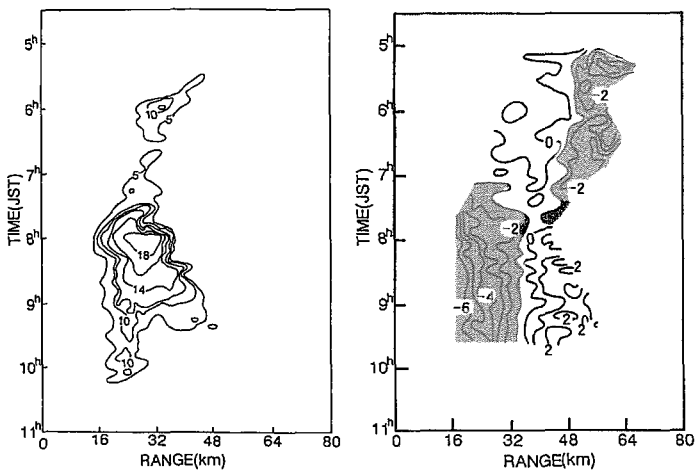

Fig. 11. Time-range cross sections of echo intensity at 1.0 km height (a) and horizontal wind speed at a height of 1.25 km (b) within the box of Fig. 9. Weaker wind regions than the time-averaged wind speed are shaded.

30. The eastern boundary of the radar echo retreated from X=48 km to 32 km between 05: 30−07:30. The radar echo became strong at 07:30, peaked in intensity at 08:00 but then weakened. The radar echo continued near the coast until 10:20. Figure 11b shows a time-range cross-section of horizontal wind speed at a height of 1.25 km. Here, "wind speed magnitude" is the deviation from the time-averaged wind speed at a height of 1.25 km. The radar echoes were weak before 07:30 when the wind speeds at X>40 km (upwind) were larger than those at X< 40 km. The radar echoes strengthened after 07:30, when wind speeds at X>32 km were larger than those at X<32 km. It is an interested feature that wind speed near the coast (X<32 km) was relatively small when the speed off the coast (X>32 km) was relatively large, and vice versa.

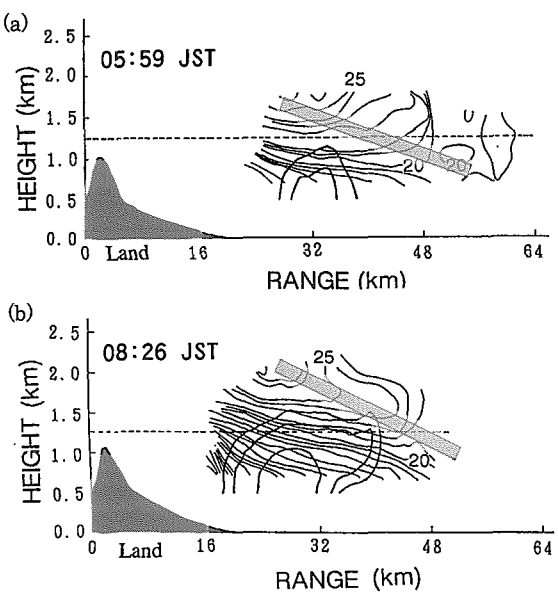

Fig. 12. Vertical cross sections of the radar echo intensity and horizontal wind speed at 05:59 and 08:26 JST within the box in Fig. 9.

Vertical cross sections of the radar echo intensity and horizontal wind speed at 05:59 and 08:26 within the box in Fig. 9 are shown in Fig. 12. The dotted line indicates a height of 1.25 km. The layer of weak winds (e.g. less than 19 m s^{-1}) was deeper and the radar echo top was higher at 08:26 than at 05:59, which is why the horizontal wind speed at a height of 1.25 km was greater prior to 07:30. The slope of the boundary between the lower, weaker winds and the upper environmental airflow was steeper at 08:26 than at 05:59. The largest echo intensities were much closer to the coast at 08:26 than at 05:59. As shown above, the depth of the blocked airflow and the slope of the boundary increased with increasing the speed of upstream wind, indicating that updraft velocity of the upper environmental airflow increased with increasing the speed of upstream wind. These features are discussed in the next section.

V. Discussion

The flow regime of a shallow fluid over an obstacle is characterized by Froude number ($Fr=U/NH$ or $Fr=U/Nh_m$, where U is the mean upstream flow speed, N is the dry or moist Brunt-Väisälä frequency, h_m is the characteristic barrier height and H is the depth of shallow fluid), and the non-dimensional obstacle height (h_m/H) (e.g., Baine, 1987; Durran and Klemp, 1982; Pierrehumbert and Wyman, 1985; Saito, 1992). These theoretical and laboratory experiments assume inviscid, hydrostatic and uniformity of wind speed and direction. Even though the applicability of the flow regime to the real atmosphere is limited, Froude number would be possibly a measure to characterize the orographic clouds and precipitation as indicated by Houze et al. (2001). Many studies indicate that the blocked airflow would be clearly observed in a stable atmosphere (Baines, 1987; Pierrehumbert and Wyman, 1985; Saito, 1992; Houze et al., 2001; Medina and Houze, 2003).

The values of H and h_m are not determined uniquely, but roughly estimated from Figs. 1 and 7. In our case, $N=0.013$ s^{-1} (dry) or 0.006 s^{-1} (moist), $U=20$ ms^{-1}, $H=2000$ m, and $h_m=1000$ m, then $Fr(dry)=0.8$ (U/NH) or 1.5 (U/Nh_m) and $Fr(moist)=1.7$ (U/NH) or 3.3 (U/Nh_m). The flow regime with these values is partially blocked without lee jump (Baines, 1987). In the case of Kanada et al. (2000), Fr(dry) is also 0.8 or 1.5, but N(moist) and Fr(moist) cannot be calculated due to neutral or unstable atmospheric stratification. These values are much larger than those of Hawaiian Rainband Project ($Fr=0.17-0.41$) (Carbone et al., 1998) and Taiwan Area Mesoscale Experiment ($Fr=0.2-0.4$). During IOP of the Mesoscale Alpine Programme (MAP) the flow was unstable with $Fr>1$, but stable with $Fr<1$ during IOP8 (Medina and Houze, 2003). When $Fr<1$, the precipitation was enhanced 140 km or more upstream of the terrain (Houze et al., 2001). Rossby radius of deformation ($L_R=Nh_mf^{-1}$,

where N is the moist Brunt-Väisälä frequency, and f is the Coriolis parameter) characterizes the horizontal scale over which the effects of blocking occur (Pierrehumbert and Wyman, 1985). Considering the space and temporal inhomogeneity of terrain and atmospheric conditions, the horizontal extent of the observed blocked air (~45 km) is not inconsistent with L_R (~80 km; $N=0.006\ s^{-1}$, $h_m=1000m$, $f=0.73\times10^{-4}s^{-1}$ for 35 °N latitude).

The maximum radar echo intensity was about 10 km off the coast. The mean slope of this interface was about 2.5 degrees, which causes vertical wind with $\sim1ms^{-1}$ when the horizontal speed of upward wind is 20 ms^{-1}. Orography affected the wind fields more than 45 km off the coast. Upward air motion was the strongest around 20 km off the coast. The presence of downward air motion was suggested near the coast. As stated above, the depth of the blocked airflow and the slope of the boundary increased with increasing the speed of upstream wind, indicating that updraft velocity of the upper environmental airflow increased with increasing the speed of upstream wind. The results from numerical simulations were used to determine whether the observed wind features were qualitatively consistent with a simulated blocked airflow. We shall show our results of numerical simulations for the convenience for explanation, although they are nothing different from those done by Saito et al. (1994).

The Advanced Regional Prediction System (ARPS) model (Xue et al., 1995) was used. The domain consisted of 120 grid points 2 km apart in both the x and y directions. There were 30 grid points in the z direction, with a vertical spacing of 400 m at each level, except for 200 m at the lowest level. The model was run under dry condition, because we are interested in the structure of the blocked airflow formed in downwind side of approaching convective clouds, thus before heavy rainfall occurs. The initial conditions were derived from upper air sounding data at Shionomisaki at 09:00 on 7 October 1993 (see Figs. 6 and 7) (SND-case). The effect of wind speed on the blocked airflow was gauged from the results of two simulations with the same conditions as the SND-case, except from the use of a vertically homogeneous wind. For the "U-10 case," the wind was $u=-10\ m\ s^{-1}$, and $v=0$; for the "U-20 case," the wind was $u=-20\ ms^{-1}$ and $v=0$. The results are shown for 7.5 hours of model time, by which time the model airflow had reached a nearly steady state.

Figure 13 shows the horizontal distributions of wind vectors and wind speed at a height of 600 m. Same with the results of earlier simulations by other researchers (e.g., Pierrehumbert and Wyman, 1985; Saito et al., 1994), the location of the weaker wind, i.e., the blocked airflow, retreats towards the coastline as wind velocity increases. Changes in wind speed at a height of 200 m are shown in Figs. 14 and 15, which show vertical cross sections of the hrizontal wind speed along the thick line in Fig. 13 ($Y=135$ km). The horizontal extent of

the blocked airflow increases as wind speeds decrease. However, the horizontal gradient of wind speed and the vertical extent of the blocked airflow increase with increasing wind speed near the coast, yielding a stronger updraft.

Wind speed does not monotonically decrease with decreasing distance from mountains; wind speeds are higher downwind of the blocked airflow. These strong winds may be mesoscale "mountain-parallel" or "barrier" jets (Schwerdtfeger, 1975; Parish, 1982; Marwitz, 1987) that can be attributed to the 3D effect of the mountain. The model wind field indicates the presence of divergence and an associated downdraft in the downwind side of the blocked airflow (not shown), which would explain the observed lowering of radar echo tops in Fig. 10. Such divergence and its associated downdraft may also explain why convective clouds dissipate rapidly just after landfall, confining heavy rainfall to the vicinity of the coast. The rapid dissipation of precipitating clouds is indispensable for the successive formation of new convective clouds as suggested by Takeda and Takase (1980).

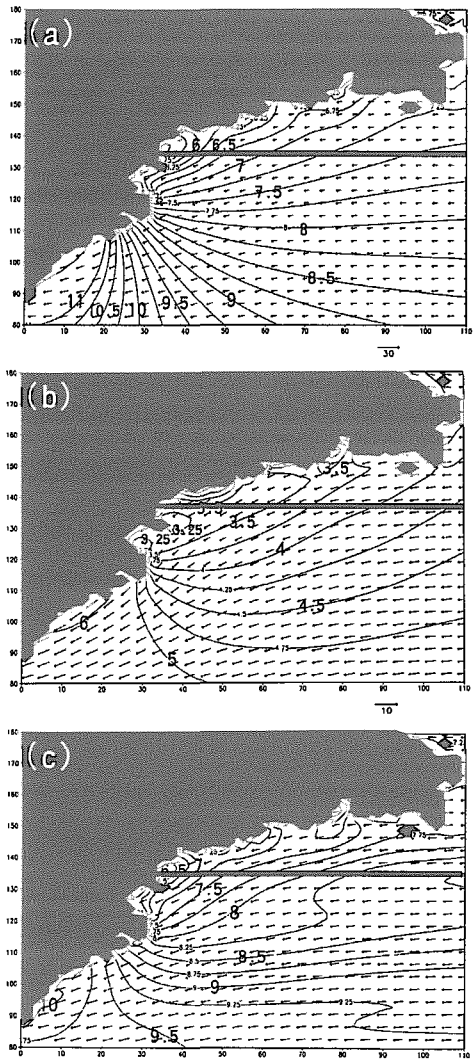

Fig. 13. Horizontal distributions of simulated wind vectors and wind speed at a height of 600 m. (a) SND case (b) U-10 case (c) U-20 case

In this case there was strong wind shear below a height of 1 km (Fig. 6). Vertical wind shear may not affect the structure of the blocked airflow itself as shown in Figs. 13 and 14. However, vertical wind shear may play an important role in the formation and dynamic structure of convective clouds in a convectively unstable atmosphere. Takeda and Takase (1980) pointed out that the vertical wind shear plays an important role for the formation of low-level convective clouds that form repeatedly over the same area offshore. That is, a downdraft is formed in the upstream of a previously developed cloud under the upshear wind field. It enhances convergence and

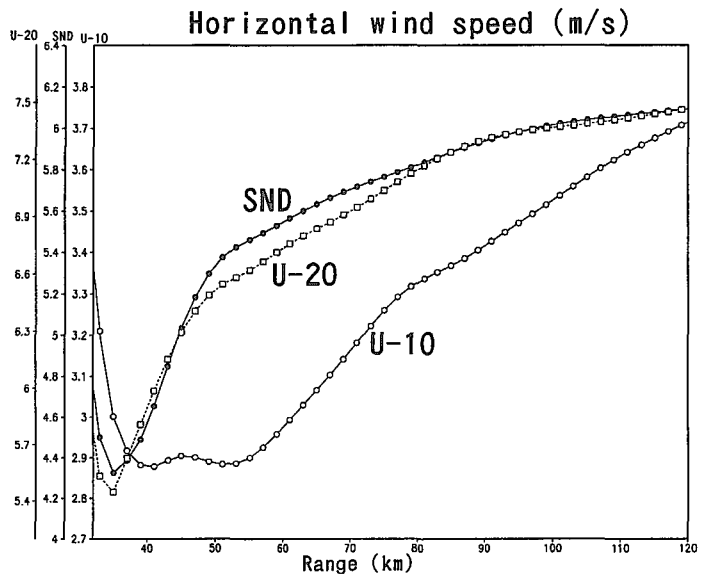

Fig. 14. Changes in simulated horizontal wind speed at a height of 200 m along the thick line in Fig. 13 (Y=135 km).

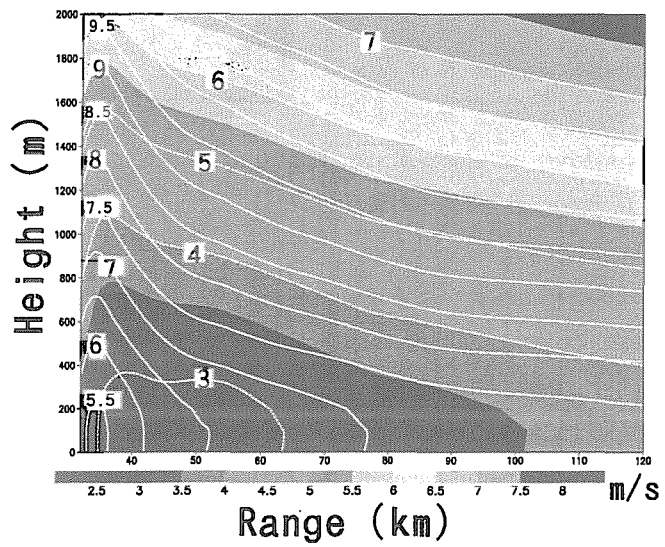

Fig. 15. Vertical cross section of the simulated horizontal wind speed along the thick line in Fig. 13 (Y=135 km). U-10 (shaded and dotted line) and U-20 (solid line)

triggers the formation of a new convective cloud in the upstream of a previously developed cloud. Evaporation of raindrops and melting of snow (i.e., cooling) also enhance blocked airflow (e.g., Bousquet and Smull, 2003; Carbone et al., 1998; Chu and Lin, 2000; Marwitz, 2003). Fujiyoshi and Takeda (1980) found cooling of low-level air owing to melting snow at Owase. Sublimation of snow particles is another important factor to maintain the sharp convergence line that affects the formation, maintenance and transformation of the snow clouds in the coastal region facing the Sea of Japan (e.g., Fujiyoshi et al., 1988; Yoshihara et al., 2004). Of course, these processes are not relevant to the present case.

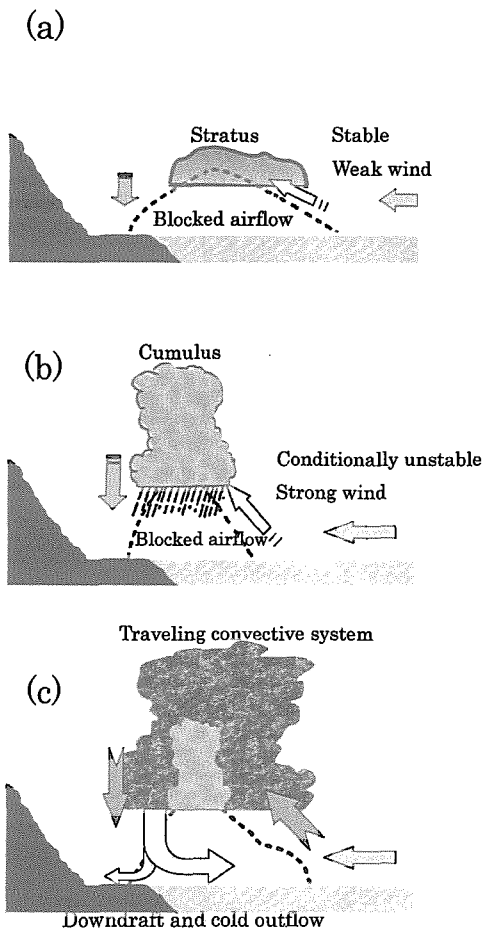

Fig. 16. A sketch of the formation of clouds associated with the blocked airflow. (a) Stratus cloud in a stable atmosphere and weak wind. (b) Cumulus cloud in a conditionally unstable atmosphere and strong wind. (c) Positive feedbacks among traveling convective system, blocked airflow, and orographically induced cumulus cloud.

VI. Concluding remarks

Many observational studies over the southeastern Kii Peninsula have suggested that mesoscale convergence of blocked airflow is responsible for heavy rainfall. However, the 3D wind fields of the blocked airflow had not been reported prior to the deployment of a dual-Doppler radar system from June to October, 1993. During this period, stratiform-type radar echoes formed in a stable atmosphere. Blocked airflow extended about 45 km offshore and was 2 km deep near the coast; the depth decreased offshore with increasing distance from the coast. An increase in the vertical extent of the blocked airflow and a decrease in the horizontal extent accompanied an increase in environmental wind speed. These observed 3D structures of blocked airflow are consistent with simulations by a 3D mesoscale numerical model (ARPS). Numerical simulations suggest the formation of a barrier jet and its associated downdraft downwind of the blocked airflow.

Figure 16 schematically summarizes the observed and simulated results. When the

low-level flow is stable and weak, the shallow blocked airflow extends about 45 km off the coast. If the air is moist enough, a low-level stratus cloud would be formed off the sea coast along the slope of the blocked airflow (Fig. 16a and C-type in Fig. 3). When the wind speed of low-level flow becomes large, the horizontal extent of the blocked airflow decreases and the vertical extent increases. If the air is moist and conditionally unstable, shallow cumulus clouds would develop easily along the slope of the blocked airflow (Fig. 16b). The micro-physical interaction between a traveling convective system and small clouds would cause heavy rainfall (Fig. 16c and L-type in Fig. 2b). The presence of divergence and an associated downdraft in the downwind side of the blocked airflow would cause rapid dissipation of precipitating clouds and strong downdraft which is indispensable for the successive formation of new convective clouds (Fig. 16c).

Based on the results of numerical simulations of Saito et al. (1994), Kanada et al. (2000) and this study, low-level convergence due to upstream blocking would commonly form under various atmospheric conditions when the mean low-level flow is easterly ~south-easterly. Therefore, the same 3D structures of the blocked airflow with those presented here are expected to be found even in heavy rainfall events.

Acknowledgement The authors would like to express our great appreciation to the Nagoya Meteorological Observatory for the supply of PPI radar-echo data. Special thanks are given to Dr. B. Geng, Dr. N. Yoshimoto, Dr. S. Kanada and Mr. M. Mori for their assistance in dual-Doppler radar observations. GrADS was used for graphics. This study was financially supported by the Scientific Research Fund from the Ministry of Education, Science, Sports and Culture.

References

Baines, P. G., 1987. Upstream blocking and airflow over mountains, *Ann. Rev. Fluid Mech.*, **19**, 75−97.

Bousquet, O. and B. F. Smull, 2003. Observations and impacts of upstream blocking during a widespread orographic precipitation event, *Quart. J. Roy. Meteor. Soc.*, **129**, 391−409.

Browning, K. A. and R. Wexler, 1968. The determination of kinematic properties of a wind field using Doppler radar, *J. Appl. Meteor.*, **7**, 105−113.

Carbone, R., W. A. Cooper and W-C Lee, 1995. Forcing of flow reversal along the windward slopes of Hawaii, *Mon. Wea. Rev.*, **123**, 3466−3480.

Carbone, R. E., J. D. Tuttle, W. A. Cooper, V. Grubisic and W. C. Lee, 1998. Trade wind rainfall near the windward coast of Hawaii, *Mon. Wea. Rev.*, **126**, 2847− 2863.

Chu, C-M. and Y-L Lin, 2000. Effects of orography on the generation and propagation of mesoscale convective systems in a two-dimensional conditionally unstable flow, *J. Atmos. Sci.*, **57**, 3817−3837.

Durran, F. R. and J. B. Klemp, 1982. On the effect of moisture on the Brunt Vaisalla frequency. *J. Atmos. Sci.*,

39, 2152−2158.

Fujiwara, M., J. Aoyagi, J. Shiino and T. Yanase, 1974. On the cloud structure related to heavy rainfall as revealed by radar, *Pap. Meteor. Geophys.*, **25**, 24−50.

Fujiyoshi, Y. and T. Takeda, 1980. Bright bands found our at different two levels simultaneously, *Tenki*, **27**, 29−34 (in Japanese).

Fujiyoshi, Y., K. Tsuboki, H. Konishi and G. Wakahama, 1988. Doppler radar observation of convergence band cloud formed on the west coast of Hokkaido Island (I): warm frontal type, *Tenki*, **35**, 427−439 (in Japanese).

Fujiyoshi, Y., 1992. Snowfall and topography, Meteorology of the water cycle, in *Lectures of Meteorology 3* (T. Asai and T. Matsuno ed.). University of Tokyo Press, 41−58 (in Japanese).

Fujiyoshi, Y., T. Fujita, T. Takeda, T. Kojiri, T. Takara and S. Ikeda, 1996. The effect of complex terrain on the leeside distribution of snowfall −In the case of Nobi Plain−, *Tenki*, **43**, 391−408 (in Japanese).

Fujiyoshi, Y., N. Yoshimoto and T. Takeda, 1998. A dual-Doppler radar study of longitudinal-mode snowbands. Part I: A three-dimensional kinematic structure of meso-.−scale convective cloud systems within a longitudinal-mode snowband, *Mon. Wea. Rev.*, **126**, 72−91.

Houze, Jr., R. A., N. J. Curtis and S. Medina, 2001. Radar observations of precipitation and airflow on the Mediterranean side of the Alps: Autumn 1998 and 1999, *Quart. J. Roy. Meteor. Soc.*, **127**, 2537−2558.

Kanada, S., B. Geng, N. Yoshimoto, Y. Fujiyoshi and T. Takeda, 1999. Doppler radar observation on the orographic modification of a precipitating convective cloud in its landing, *J. Meteor. Soc. Japan*, **77**, 135−154.

Kanada, S., H. Minda, B. Geng and T. Takeda, 2000. Rainfall enhancement of band-shaped convective cloud system in the downwind side of an isolated island, *J. Meteor. Soc. Japan*, **78**, 47−67.

Kawashima, M. and Y. Fujiyoshi, 2005. Shear instability along a snowband: Instability structure, evolution, and energetics derived from dual-Doppler radar data, *J. Atmos. Sci.*, **62**, 351−370..

Kodama, Y., M. Maki, S. Ando, M. Otsuki, O. Inaba, J. Inoue, N. Koshimae, S. Nakai and T. Yagi, 1999. A weak-wind zone accompanied with swelled snow clouds in the upstream of a low-altitude ridge − Single Doppler radar observations over the Tsugaru district of Japan−, *J. Meteor. Soc. Japan*, **77**, 1039−1059.

Kuo, Y-H. and G. T-J Chen, 1990. The Taiwan area mesoscale experiment (TAMEX): An overview, *Bull. Am. Meteorol. Soc.*, **71**, 488−503.

Marwitz, J. D., 1987. Deep orographic storms over the Sierra Nevada. Part I: Thermodynamic and kinematic structure, *J. Atmos. Sci.*, **44**, 159−173.

Medina, S. and R. A. Houze Jr, 2003. Air motion and precipitation growth in Alpine storms, *Quart. J. Roy. Meteor. Soc.*, **129**, 345−371.

Nakai, S., M. Kajikawa and Y. Yamada, 1998. The relation between prevailing precipitation-particle type and radar echo structure around the Dewa Hills, *Atmos. Res.*, **47−48**, 97−112.

Parish, T., 1982. Barrier winds along the Sierra Nevada mountains, *J. Appl. Meteor.*, **12**, 925−930.

Pierrehumbert, R. T. and B. Wyman, 1985. Upstream effects of mesoscale mountains, *J. Atmos. Sci.*, **42**, 977−1003.

Saito, K., 1992. Shallow water flow having a lee hydraulic jump over a mountain range in a channel of variable width, *J. Meteor. Soc. Japan*, **70**, 775−782.

Saito, K., M. Murakami, T. Matsuo and H. Mizuno, 1994. Sensitivity experiments on the orographic snowfall over the mountainous region of northern Japan, *J. Meteor. Soc. Japan*, **74**, 797−813.

Saito, K., L. Thanh and T. Takeda, 1994. Airflow over Kii peninsula and its relation to the orographic enhancement of rainfall, *Pap. Meteor. Geophys.*, **45**, 65−90.

Sakakibara, H. and T. Takeda, 1973. Modification of Typhoon 7002 rainfall by orographic effect, *J. Meteor.*

Soc. Japan, **51**, 155−167.

Sakakibara, H., 1981. Heavy rainfall from very shallow convective clouds, *J. Meteor. Soc. Japan*, **59**, 387−394.

Schwerdtfeger, W., 1975. The effect of the Antarctic Peninsula on the temperature regime of the Weddell Sea, *Mon. Wea. Rev.*, **103**, 45−51.

Seko, H., T. Kato, K. Saito, M. Yoshizaki, K. Kusunoki, M. Maki, and Members of Tsukuba Area Precipitation Studies, 1999. Analytical and numerical studies of a quasi-stationary precipitation band observed over the Kanto area associated with typhoon 9426 (Orchid), *J. Meteor. Soc. Japan*, **77**, 929−948.

Shiino, J., 1976. On convective clouds at Owase in the cases of heavy rain −A study by one-dimensional model of cumulus convection−, *J. Meteor. Soc. Japan*, **54**, 407−426.

Smull, B. F., O. Bousquet and D. Luthi, 2001. Evaluation of real-time MC2 simulation results for a case of significant upstream blocking during MAP, 84−87 in *MAP Newsletter No.15*. MeteoSwiss, CH-8044, Zurich, Switzerland.

Staff Members of Tokyo University, 1969. Precipitation bands of typhoon Vera in 1959 (Part I), *J. Meteor. Soc. Japan*, **47**, 298−309.

Staff Members of Tokyo University, 1970. Precipitation bands of typhoon Vera in 1959 (Part II), *J. Meteor. Soc. Japan*, **48**, 103−117.

Takeda, T., N. Moriyama and Y. Iwasaka, 1976. A case study of heavy rain in Owase area, *J. Meteor. Soc. Japan*, **54**, 32−41.

Takeda, T. and K. Takase, 1980. Radar observation of rainfall system modified by orographic effects, *J. Meteor. Soc. Japan*, **58**, 500−516.

Xue, M., K. Droegemeier, V. Wong, A. Shapiro, and K. Brewster, 1995. *Advanced Regional Prediction System (ARPS) Version 4.0 user's guide*. Center for Analysis and Prediction of Storms, University of Oklahoma, 320 pp.

Yanagisawa, Z., J. Aoyagi and N. Kamibayashi, 1974. Radar analysis on the precipitation around Owase, *Pap. Meteor. Geophys.*, **25**, 51−80.

Yoshihara, H., M. Kawashima, K. Arai, J. Inoue and Y. Fujiyoshi, 20004. Doppler radar study on the successive development of snowbands at a convergence line near the coastal region of Hokuriku district, *J. Meteor. Soc. Japan*, **82**, 1057−1079.

紀伊半島南東沖に形成された風上弱風域のドップラーレーダ観測

藤吉　康志
北海道大学低温研究所・海洋研究開発機構地球環境フロンティア研究センター
田中　久理*
名古屋大学大気水圏科学研究所
川島　正行
北海道大学低温研究所
圓山　憲一
独立行政法人防災科学技術研究所
武田　喬男
名古屋大学・名誉教授

(2004年12月3日受理)

積乱雲は，地形の影響によってさまざまな影響を受け，局地的な豪雨をもたらす．特に紀伊半島の南東部は，日本有数の豪雨地帯であり，多くの研究者によって地形性豪雨の研究がなされてきた．その結果，地形によってブロックされた気流が沖合に作る収束場が，上陸直前の雲の発達および，長時間停滞する降水バンドの形成に重要であることが指摘されてきた．しかし，これまで海上の収束場を観測的に確認することはできなかった．そこで我々は，1993年6月～10月まで，2台のドップラーレーダを紀伊半島の東に設置して，降水雲と海上の風の3次元分布観測を行った．その結果，移動性の降水システムが上陸する前に海上で一旦発達し，それが，海上に形成された地形性の収束場の影響による可能性を指摘した（Kanada et al., 1999）．しかし，このように発達した積乱雲の場合には，それ自身が周囲の気流場を変形させてしまうため，純粋に地形性の収束場を抽出することはできなかった．

一方，雲システムが接近する前に，どのような厚さと広がりを持った弱風域が形成されるのかを明らかにすることは，これらの雲システムが地形によってどのように発達あるいは変質するかを予測する上で重要な要素である．この観測期間中の10月7日，沖合海上に背の低い弱いエコーが約7時間以上にわたって停滞した．我々は，この観測事例を詳細に調べることにより，強い対流性の雲システムが接近する前に山の風上沖合に形成される弱風域の3次元構造を世界で初めて明らかにした．すなわち，弱風域は，海岸から沖合45 kmまで広がっていた．弱風域は海岸近くでは厚さが約2 kmあったが，沖合に行くにつれて次第に薄くなり，その勾配は約2.5度であった．沖合の一般風の風速が大きくなるにつれて，弱風域は狭くなると同時に厚くなった．これらの観測事実は，数値モデルによる再現および感度実験の結果と整合的であった．

*現在所属：三菱電機（株）